X-621-72-495

PREPRINT

THE EFFECT OF GRID TRANSPARENCY AND FINITE COLLECTOR SIZE ON DETERMINING ION TEMPERATURE AND DENSITY BY THE RETARDING POTENTIAL ANALYZER

B. E. TROY, JR.
E. J. MAIER

JANUARY 1973

GODDARD SPACE FLIGHT CENTER
GREENBELT, MARYLAND

THE EFFECT OF GRID TRANSPARENCY AND FINITE COLLECTOR SIZE ON DETERMINING ION TEMPERATURE AND DENSITY BY THE RETARDING POTENTIAL ANALYZER

by

B. E. Troy, Jr. and E. J. Maier

ABSTRACT

The analysis of ion data from retarding potential analyzers (RPA's) is generally done under the planar approximation, which assumes that the grid transparency is constant with angle of incidence and that all ions reaching the plane of the collectors are collected. These approximations are not valid for situations in which the ion thermal velocity is comparable to the vehicle velocity, causing ions to enter the RPA with high average transverse velocity. To investigate these effects, we calculate current-voltage curves for H^+ at 4000° K, taking into account the finite collector size and the variation of grid transparency with angle. These curves are then analyzed under the planar approximation. The results show that only small errors in temperature and density are introduced for an RPA with typical dimensions; and that even when the density error is substantial for non-typical dimensions, the temperature error remains minimal. This last fact may be useful for designing a non-typical RPA which is optimized to operate in unusual conditions.

CONTENTS

One of the primary instruments for making direct measurements on charged particles in the earth's ionosphere has been the retarding potential analyzer (RPA). RPA's have been flown on rockets, satellites and space probes to determine electron density and temperature, and positive ion density, temperature and mass number (Serbu and Maier, 1966; Maier, 1969; Chandra et al., 1970).

A typical planar RPA is represented in Figure 1, with (for example) three grids G_1, G_2, and G_3, and a current collector C. The aperture radius is r, the collector radius is R, and the interelement spacings are d_1, d_2, and d_3. Charged particles entering the aperture and reaching C are collected as a measured current I. For ion measurements, constant voltages applied to G_1, G_3, and C repel the electrons and accept the ions, so that I consists of only ions. A varying ion retarding potential V is applied to G_2, so that I is a function of V. Further details of RPA operation may be found elsewhere (Knudsen, 1966; Donley, 1969).

The parameters to be measured are then obtained by fitting a theoretical curve to a large number of experimental data points comprising the collected current versus retarding voltage curve, or I-V curve. This fitting process is generally more involved for ions than for electrons, since more than one ionic species may be present, and the resulting I-V curve is the sum of the individual I-V curves for the several species. Despite this complication, programs have been developed which can deduce the ion temperature and the individual densities from either simple one-component curves or from multi-component curves

(Moss and Hyman, 1968; Patterson, 1969). In these analysis programs, the I-V curve is assumed to obey the following formula, written here for multiple ion species:

$$I = \sum_i I_i,$$

$$I_i = (\pi r^2)\,\tau^3\, e\, N_i\, v_s \cos a \left[\frac{1}{2} + \frac{1}{2}\,\mathrm{erf}\,(s-t) + \frac{1}{2\sqrt{\pi}\, s}\, e^{-(s-t)^2}\right] \qquad (1)$$

$$s = \frac{v \cos a}{a_i}$$

$$t = \sqrt{\frac{e\,(V-\phi_s)}{k\,T_+}}$$

v_s = satellite velocity

a = trap-velocity angle (Fig. 1)

a_i = thermal velocity of i^{th} ion species = $\sqrt{\frac{2k\,T_+}{m_i}}$

k = Boltzmann's constant

T_+ = ion temperature

m_i = mass of i^{th} ion species

e = electron charge

V = retarding potential

τ = transparency of single grid

N_i = ion density of i^{th} ion species

ϕ_s = satellite potential.

All ion species are assumed to have the same temperature T_+. A sample multi-species ion curve with theoretical fit and results is shown in Figure 2.

In the application of formula (1) to analyze ion I-V curves taken by a planar RPA, several approximations or assumptions are made:

(1) The ambient ionic velocity distribution is Maxwell-Boltzmann, i.e., characterized by a temperature T_+; and that this distribution is unchanged at the RPA aperture, except for a uniform translation due to the satellite potential.

(2) Each grid represents an equipotential plane according to the voltage applied to that grid.

(3) The percentage of ions which pass through each grid is equal to the optical transparency of that grid taken at normal incidence.

(4) Every ion which passes through all grids will hit the collector plate.

(5) The measured current is due only to ions.

In general, these approximations are not perfectly true. Consequently, the RPA should be designed and operated so as to maximize the validity of (1) - (5), or else appropriate corrections should be made for effects which cannot be "designed away."

Within the past few years, the operation of the RPA has been looked at in some detail, in order to better our understanding of its capabilities. These investigations have been undertaken for several reasons. For one, satellite-borne RPA's have been operating in altitude ranges where several ions (mainly

0^+, H^+ and He^+) must be accounted for simultaneously. Also, the large amount of data returned by satellites and ground-based research stations has given a resonably good picture of the ionosphere, so that experimenters are now concerned with accuracies of some percent, rather than orders of magnitude. Multi-experiment satellites have allowed intercomparison of results between different experimental methods. In addition, there have been disagreements between satellite experiments and radar backscatter experimenters over ionospheric temperatures (Hanson et al., 1969; McClure and Troy, 1971).

Some of the previously listed approximations under which RPA analysis occurs have been checked by different investigators: Whipple and Parker (1970) have considered the first approximation, and concluded that the ion I-V curve is minimally affected when the Debye length is small. The second approximation, that the grids are perfect equipotential planes, has been investigated by Knudsen (1966), Hanson et al., (1972), Golden et al., (1972) and Whipple et al., (1972). The last three assumptions were discussed by Whipple et al., (1968), but only relative to high energy isotropic particles which pass through the RPA grids unaffected by the grid voltages, i.e., not for the I-V curve. RPA theory for electrons has also been dealt with by Whipple and Parker (1969 a & b).

It is the purpose of this paper to investigate the effects of grid transparency and finite collector size (approximations 3 and 4) on the determination of thermal ion density and temperature from I-V curves. The procedure will be to compute

the shape of the I-V curve for given conditions (RPA dimensions, grid configuration, ion temperature and density, etc.), and then analyze the curve by the existing method. The differences between the assumed temperature-density values and the analyzed values will represent the magnitude of the error introduced by the grid transparency and finite collector effects. These results will not include the effect of grid plane potential non-uniformities (Whipple et al., 1972).

FINITE COLLECTOR EFFECT

Figure 3 illustrates the geometry used for determining the current to the collector. An ion of mass m_i and velocity v arrives at the center of the aperture at polar angle θ and azimuthal angle ϕ (see figure 3a). The ion passes through the grids (not shown) and arrives at point P in the plane of the collector. P may be either on or off the collector. The ion generally does not follow a straight path from aperture to collector, due to the effect of electric fields between the grids. However, all positive ions with the same v, θ , ϕ will follow similar paths, so that their locus in the collector plane will be a projection of the aperture, but displaced horizontally by a distance l. The projection will lie either inside the collector ($l < R-r$) so that all v, θ , ϕ ions are collected; outside the collector ($l > R+r$) with no ions collected; or athwart the collector boundary ($R+r > l > R-r$) with some fraction f being collected. For a given l, f is determined by

$$f = \frac{A(R, r, l)}{\pi r^2}$$

where A(R, r, l) is the area of the projection within the collector boundary, i.e., the intersection of the two circles.

Since R and r are predetermined constants, f may be computed if l is known. Figure 3b illustrates the method of determining l. The grids and collector are represented by potential planes, with a resulting electric field $\vec{E}$ between the planes. Between any two planes, $\vec{E}$ is assumed to be constant in magnitude and direction:

$$\vec{E}_j = -\frac{V_j - V_{j-1}}{d_j}\vec{n}$$

where $\vec{n}$ is a unit vector normal to the potential planes.

An ion enters this field at an angle θ_{j-1} and velocity v_{j-1}. Its velocity parallel to the planes is unaffected, but its velocity normal to the planes changes depending upon E. The ion then passes plane j at an angle $\theta_j \neq \theta_{j-1}$ and velocity $v_j \neq v_{j-1}$, having traversed a horizontal distance l_j (see fig. 3b). The values of θ_j, v_j and l_j can be computed from θ_{j-1} and v_{j-1} by simple mechanics. This calculation is done sequentially for all intervals d_j between the aperture and the collector, each ion entering the aperture with its ambient values of θ and v.

The value of l is then determined by summing l_j for all intervals:

$$l = \sum_j l_j.$$

For a given ion mass and a given RPA configuration, l will depend on θ and v, but

will be independent of ϕ. Therefore, the fraction f will be a function of θ and v:

$$f = f(\theta, v).$$

The physical effect of the finite collector size will be dealt with in the calculation of I by using an effective aperture area of $\pi r^2 f(\theta, v)$, instead of the constant area πr^2.

TRANSPARENCY EFFECT

The transparency of a square wire mesh grid has been derived by Whipple et al., (1968):

$$\tau(\theta, \phi) = \left[1 - \frac{b}{a}\sqrt{1 + \tan^2\theta \cos^2\phi}\right]\left[1 - \frac{b}{a}\sqrt{1 + \tan^2\theta \sin^2\phi}\right],$$

where b is the wire diameter, a is the wire spacing and θ, ϕ are the ion angles at the grid (Fig. 3a). Since $\tau(\theta, \phi)$ is not strongly dependent on ϕ, one can determine an average transparency (θ) by integrating over ϕ:

$$\tau(\theta) = \frac{2}{\pi}\int_0^{\frac{\pi}{2}} \tau(\theta, \phi)\, d\phi.$$

The full expression is given by Whipple et al., (1968).

The transparency at each grid plane j is then given by $\tau(\theta_j)$, instead of the normal transparency $\tau = \tau(0)$ used in equation (1). The value of θ_j depends upon the ambient θ, v of the ion before it passes the first grid. Therefore, we relable $\tau(\theta_j)$ as $\tau_j(\theta, v)$. The total transparency for an n-grid trap is then $\prod_{j=1}^{n} \tau_j(\theta, v)$ rather than $\tau^n(0)$.

CALCULATION OF THE ION I-V CURVE

We can now incorporate the area factor $f(\theta, v)$ and the transparency $\tau_j(\theta, v)$ into our calculation of the I-V curve. The standard I-V curve, equation (1), is calculated by integration over the velocity distribution function:

$$I = \pi r^2 e \tau^n(0) \frac{N_+}{\pi^{3/2} a^3} \int_{-\infty}^{\infty} dv_x \int_{-\infty}^{\infty} dv_y \int_{v_{min}}^{\infty} dv_z \, v_z \, e^{-\frac{1}{a^2}\left[(v_x - v_{sx})^2 + (v_y - v_{sy})^2 + (v_z - v_{sz})^2\right]}$$

where v_{min} is determined by the retarding potential, and v_{sx}, v_{sy}, v_{sz} are the components of v_s in the RPA frame of reference. Changing to polar coordinates, we have:

$$I = \pi r^2 e \tau^n(0) \frac{N_+}{\pi^{3/2} a^3} \int_0^{\frac{\pi}{2}} d\theta \int_{v_{min}}^{\infty} dv \int_0^{2\pi} d\phi \, v^3 \sin\theta \cos\theta \, e^{-\frac{g(\theta,\phi)}{a^2}},$$

$g(\theta, \phi) = v^2 + v_s^2 - 2v v_s [\cos\alpha \cos\theta + \sin\alpha \sin\theta (\sin\beta \sin\phi + \cos\beta \cos\phi)]$, where α, β are the angles in polar coordinates for the velocity vector v_s. Now we replace the area πr^2 by $\pi r^2 f(\theta, v)$, and $\tau^n(0)$ by $\prod_{j=1}^{n} \tau_j(\theta, v)$. Doing this, and rearranging terms to the left, we have:

$$I = \frac{\pi r^2 N_+ e}{\pi^{3/2}} \int_0^{\frac{\pi}{2}} d\theta \sin\theta \cos\theta \int_{v_{min}}^{\infty} dv \left(\frac{v}{a}\right)^3 \prod_{j=1}^{n} \tau_j(\theta, v) f(\theta, v) \int_0^{2\pi} d\phi e^{-\frac{g(\theta,\phi)}{a^2}} \tag{2}$$

$$= \frac{\pi r^2 N_+ e}{\pi^{3/2}} \{\text{triple integral}\}.$$

Formula (2) is now integrated numerically, and compared with the analytically computed value of formula (1). For simplicity, formula (2) has been written for a single ion species. In practice, both formulas are normalized to the

ram ion current I_0, which does not depend on the retarding potential V:

$$I_0 = \pi r^2 \tau'' (0) e N_+ v_s.$$

Naming the currents from formulas (1) and (2) as I(1) and I(2) respectively, we have:

$$J(1) = \frac{I(1)}{I_0} = F(s, t) = \frac{1}{2} + \frac{1}{2} \operatorname{erf}(s - t) + \frac{1}{2\sqrt{\pi}\, s} e^{-(s-t)^2}, \tag{3}$$

$$J(2) = \frac{I(2)}{I_0} = \frac{1}{\pi^{3/2} v_s \tau'' (0)} \text{ [triple integral]}. \tag{4}$$

Both J(1) and J(2) depend on V: J(1) through the term $t = \sqrt{\frac{e(V - \phi_s)}{k T_+}}$, and J(2) through the lower limit on the velocity integral shown in formula (2). Therefore, formula (4) effectively describes the ion I-V curve including the finite collector and grid transparency effects, and formula (3) describes the I-V curve without the effects, i.e., the planar approximation.

RESULTS

As a typical RPA, we use the one flown on ISIS-2, with r = 1.27 cm, R = 3.17 cm, $d = d_1 = d_2 = d_3 = 0.5$ cm, and b/a = 0.04. To test the effect of finite collector size, runs are made varying first R, and then varying d. The effect of increasing d will be similar to the effect of decreasing R: to cause more ions to miss the collector. However, an increase in d is not perfectly equivalent to a decrease in R except for r = 0, i.e., a point aperture. The results are presented as functions of normalized parameters d/r and R/r. Next, runs are made to determine the effect of grid transparency by varying b/a. To

separate the effect of grid transparency from that of finite collector size, we set the wire parameter b/a at essentially zero (10^{-4}) while varying R/r and d/r, and we set R at essentially infinitely (10 meters) while varying b/a. All runs are made with the trap-velocity angle $\alpha = 0$.

If all ions entered the aperture at normal incidence, the planar approximation F(s,t) would perfectly describe the shape of the current-voltage curve, insofar as the effects considered in this paper are concerned. But ions entering with high θ and high v will see grid transparency different from τ (0), and will also have a chance of missing the collector. Low ion mass and high temperature will enhance the high θ and high v component of the velocity distribution. Therefore, we choose hydrogen at 4000°K. to give a reasonable upper limit on the difference between F(s,t) and J(2) for a real RPA, i.e., an upper limit on the effects we are investigating.

The accuracy of our calculation is tested by making a run with an RPA having $b/a = 10^{-4}$ and R = 10 meters, where it is expected that J(2) = F(s,t). In fact, the difference between the computed J(2) and F(s,t) for this case turns out to be less than 0.25%, which is to say that they are identical within the experimental accuracy of the RPA.

The retarding voltage array used in the calculation is one point every 0.1 volts from 0.0 to 1.7 volts, which is enough to decrease the current by an order of magnitude. This amount of decrease is about what one might realistically

expect to observe for hydrogen experimentally; therefore all our hydrogen calculations are based on a retarding voltage range of 0.0-1.7 volts.

Finite collector effect.

Figure 4 shows the variation of the computed ion temperature and density with the collector parameter R/r. Other parameters are fixed at $b/a = 10^{-4}$ and $d/r = 0.39$. The density is normalized to the value obtained from the test trap ($b/a = 10^{-4}$, R/r = 10 meters/1.27 cm = 787), and the assumed temperature is 4000°. As expected, the derived density decreases with decreasing R/r, so that there is a 30% density error when the collector is the same size as the aperture at R/r = 1. There is negligible error at the real RPA value of R/r = 3.17cm/1.27 cm = 2.5.

The temperature, however, shows no truly significant error anywhere in the range investigated, with a maximum error of about 1% (the error bars are assigned by the computer curve-fitting routine). We are left with the interesting result that the RPA can give the correct temperature even when it is giving density with a substantial error.

The effect of varying d/r is shown in Figure 5, for a trap with $b/a = 10^{-4}$ and R/r = 2.50. The results bear out what was suggested earlier, namely that an increase in d/r is similar to a decrease in R/r. Again, the density error can be large ($d/r > 1.0$) while the temperature error is rather small. The real RPA value of d/r = 0.39 yields small errors in both density and temperature.

Grid transparency effect.

Now that we have shown that the dimensions of the sample RPA are properly chosen, we investigate the effect of varying the grid transparency by varying b/a. Figure 6 shows these results for the RPA with a large collector (R/r = 787). As with the finite collector effect in the previous section, the temperature error remains small even for moderate errors in the density. The normalized density n_+, however, shows a different dependency: n_+ decreases linearly with b/a = 0, whereas n_+ approached 1.0 asymptotically as a function of d/r and R/r (see figures 4 and 5). The density error is therefore definitely non-zero, although it is less than 10% for most ion traps (b/a = 0.04 for the sample RPA, $b/a \leq 0.1$ for most other RPA's).

It should be noted that the errors shown in the figures represent reasonable upper limits, being derived for hydrogen at 4000° K. Therefore, we check the lower limit by using oxygen at 1000° K for b/a = 0.2. The analysis results of this run (n_+ shown in Fig. 6, $T_+ = 1014 \pm 13°$ K) indicate that errors in the derived results for oxygen at 1000° K will be negligible over a reasonable range of b/a.

SUMMARY

We have investigated the effects of finite collector size and grid transparency on RPA ion data analysis under the assumptions outlined in the text. These effects result from the fact that ions generally do not enter the aperture

at normal incidence. The ions may hit the grid wires with an increased probability due to the variation of grid transparency with angle of incidence, or they may miss the collector entirely because of its finite size. Each effect decreases the current to the collector compared to that which is assumed by the planar approximation.

Several current voltage curves are calculated for a varying RPA parameters and a given ion mass, temperature and density. The curves are analyzed under the planar approximation and the resulting densities and temperatures and plotted versus the varying parameter. The differences between the given and derived temperatures and densities represent the errors due to the effects being investigated.

We find that for the dimensions of our sample RPA, the temperature and density errors are both small. The temperature error will remain small, even when the parameter is changed enough to substantially increase the density error. This information could be useful for someone designing an RPA to be used under conditions quite different from those of satellites in earth orbits. For instance, the aperture could be greatly increased for a given collector size to make measurements in low density regions. Or the grid wire size could be increased to combat heating effects during planetary probe missions. The derived temperature can be assumed correct, and the density increased according to calculations.

REFERENCES

Chandra, S., B. E. Troy, Jr., J. L. Donley, and R. E. Bourdeau, OGO 4 observations of ion composition and temperatures in the topside ionosphere, J. Geophys. Res., 75, 3867, 1970.

Donley, J. L., The thermal ion and electron trap experiments on the Explorer XXXI satellite, Proc. IEEE, 57, 1061, 1969.

Goldan, P. D., E. J. Yadlowsky, and E. C. Whipple, Experimental determination of retarding potential analyzer errors caused by potential nonuniformities in the grid plane, EOS, 53, 472, 1972.

Hanson, W. B., D. R. Frame and J. E. Midgley, Errors in retarding potential analyzers caused by nonuniformity of the grid-plane potential, J. Geophys. Res., 77, 1914, 1972.

Hanson, W. B., L. H. Brace, P. L. Dyson, and J. P. McClure, Conflicting electron temperature measurements in the upper F region, J. Geophys. Res., 74, 400, 1969.

Knudsen, W. C., Evaluation and demonstration of the use of retarding potential analyzer for measuring several ionospheric quantities, J. Geophys. Res., 71, 4669, 1966.

Maier, E. J. R., Sounding rocket measurements of ion composition and charged particle temperatures in the topside ionosphere, J. Geophys. Res., 74, 815, 1969.

McClure, J. P., and B. E. Troy, Jr., Equatorial ion temperature: a comparison of conflicting incoherent scatter and OGO 4 retarding potential analyzer values, J. Geophys. Res., 76, 4534, 1971.

Moss, S. J., and E. Hyman, Minimum variance technique for the analysis of ionospheric data acquired in satellite retarding potential analyzer experiments, J. Geophys. Res., 73, 4315, 1968.

Patterson, T. N. L., Deduction of ionospheric parameters from retarding potential analyzers, J. Geophys. Res., 74, 4799, 1969.

Serbu, G. P., and E. J. R. Maier, Low energy electrons measured on Imp-2, J. Geophys. Res., 71, 3755, 1966.

Whipple, E. C. Jr., J. W. Hirman, and R. Ross, A satellite ion-electron collector: experimental effects of grid transparency, photoemission, and secondary emission, ESSA Tech. Rept., ERL #99-AL1, 1968.

Whipple, E. C., Jr., and L. W. Parker, Theory of an electron trap on a charged spacecraft, J. Geophys. Res., 74, 2962, 1969a.

Whipple, E. C., Jr., and L. W. Parker, Effects of secondary electron emission on electron trap measurements in the magnetosphere and solar wind, J. Geophys. Res., 74, 5763, 1969b.

Whipple, E. C., E. J. Yadlowsky, and P. D. Goldan, Ion trajectory perturbations caused by potential nonuniformities in the grid plane of retarding potential analyzers, EOS, 53, 472, 1972.

FIGURE CAPTIONS

Figure 1. Schematic of the RPA, showing the aperture radius r, the collector radius R, and the trap depth $d = d_1 + d_2 + d_3$.

Figure 2. A multi-component current-voltage curve, with analysis results.

Figure 3a. The projection of the aperture image onto the collector plane by ions having specific velocity magnitude and direction.

Figure 3b. Variation of the ion path direction between two grids.

Figure 4. Variation with collector size of ion temperature and density derived from computed I-V curves for an RPA with $d/r = 0.39$ and $b/a = 10^{-4}$. All points are for H^+ at 4000° K.

Figure 5. Variation with RPA depth of ion temperature and density derived from computed I-V curves for an RPA with $R/r = 2.50$ and $b/a = 10^{-4}$. All points are for H^+ at 4000° K.

Figure 6. Variation with wire parameter b/a of ion temperature and density derived from computed I-V curves for an RPA with $R/r = 787$ and $d/r = 0.39$. The triangle is for O^+ at 1000° K.; all other points are for H^+ at 4000° K.

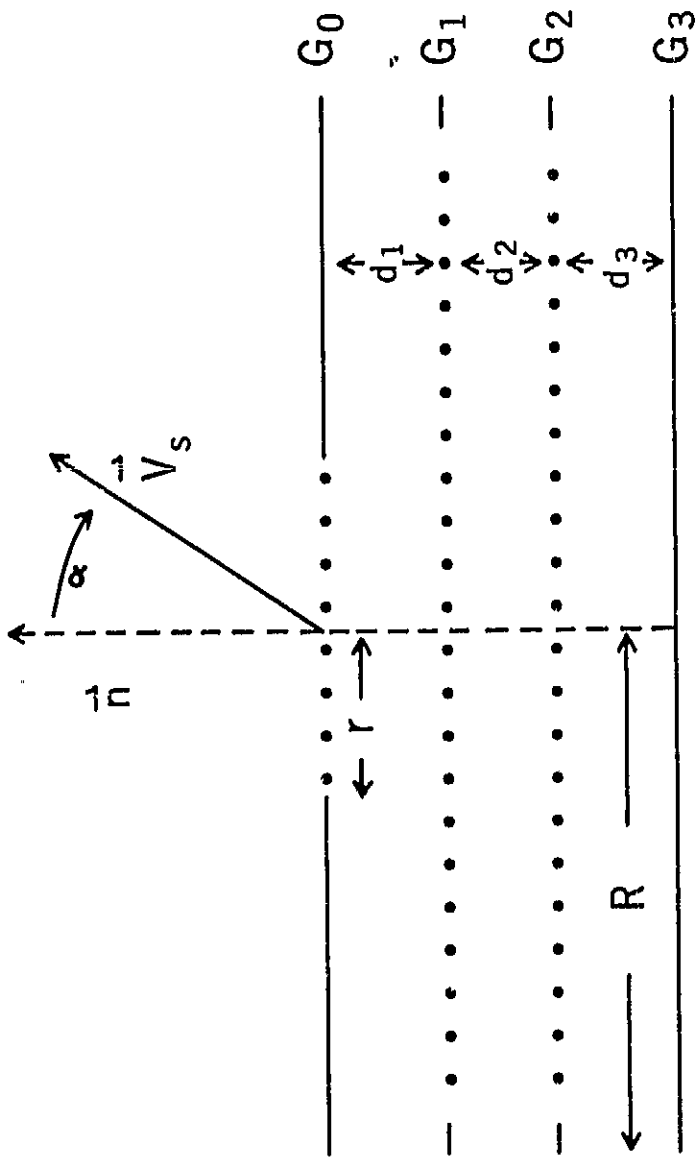

Figure 1.

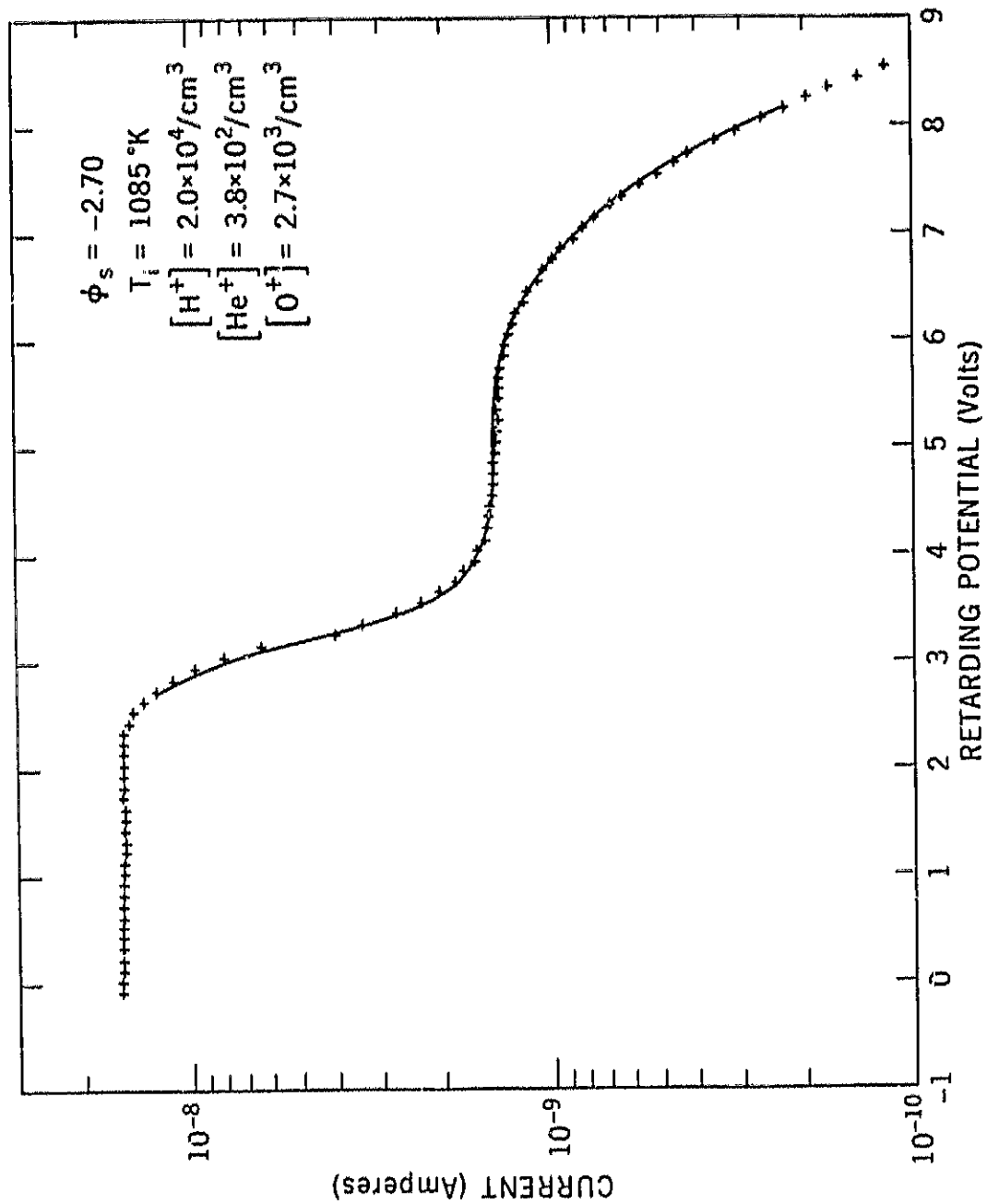
$\phi_s = -2.70$
$T_i = 1085\ ^\circ K$
$[H^+] = 2.0\times10^4/cm^3$
$[He^+] = 3.8\times10^2/cm^3$
$[O^+] = 2.7\times10^3/cm^3$
CURRENT (Amperes)
10^{-8}
10^{-9}
10^{-10}
-1
0
1
2
3
4
5
6
7
8
9
RETARDING POTENTIAL (Volts)

Figure 2.

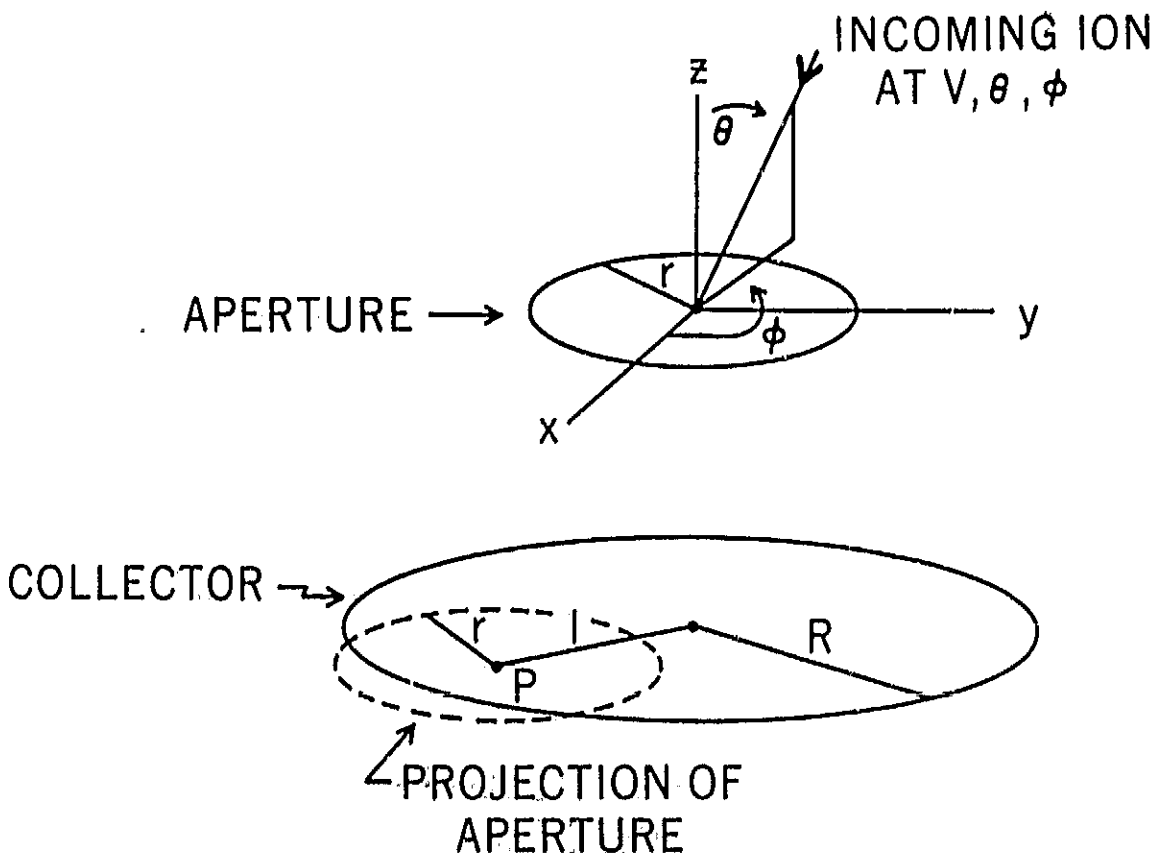

Figure 3a.

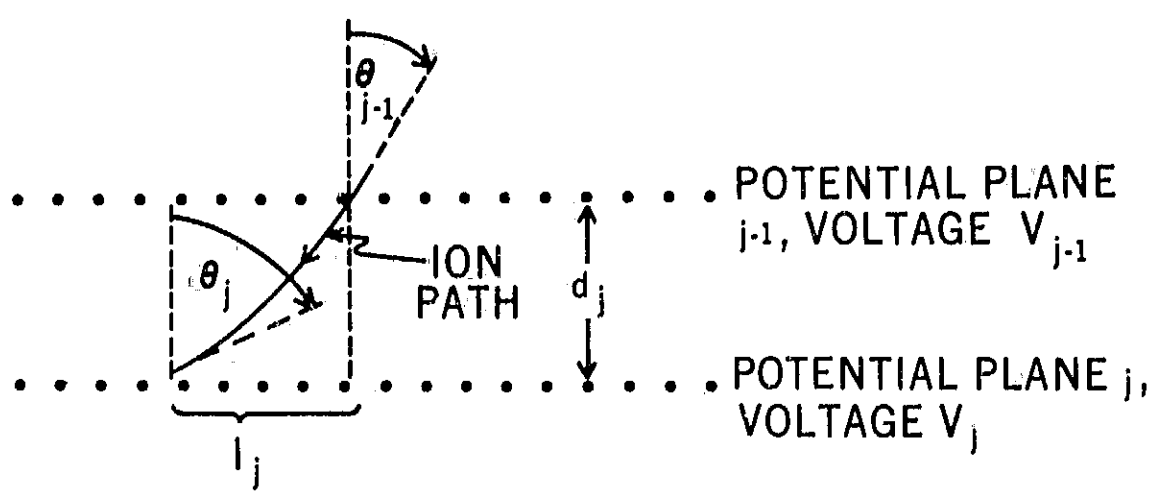

Figure 3b.

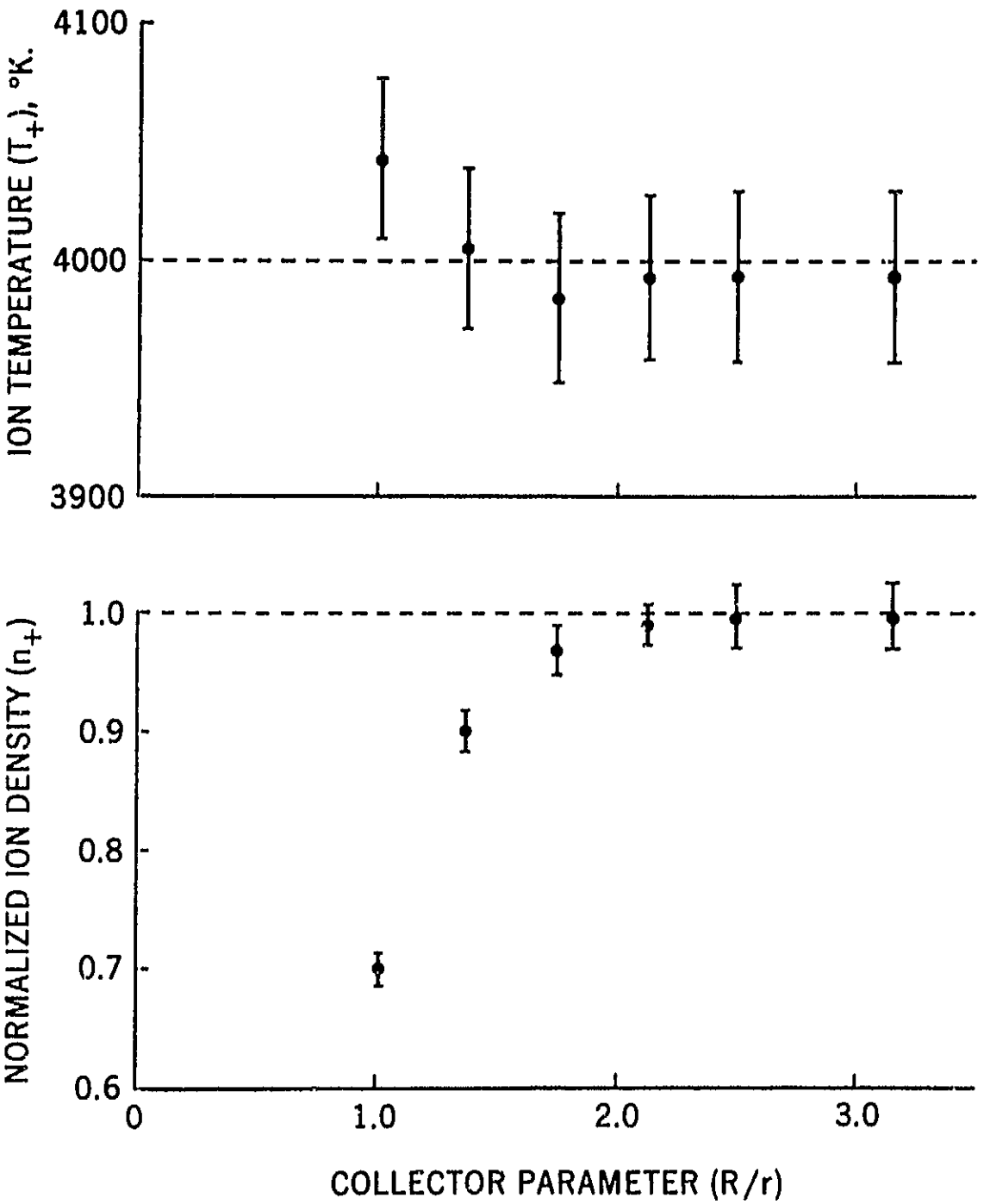
4100
4000
3900
ION TEMPERATURE (T_+), °K.
1.0
0.9
0.8
0.7
0.6
NORMALIZED ION DENSITY (n_+)
0
1.0
2.0
3.0
COLLECTOR PARAMETER (R/r)

Figure 4.

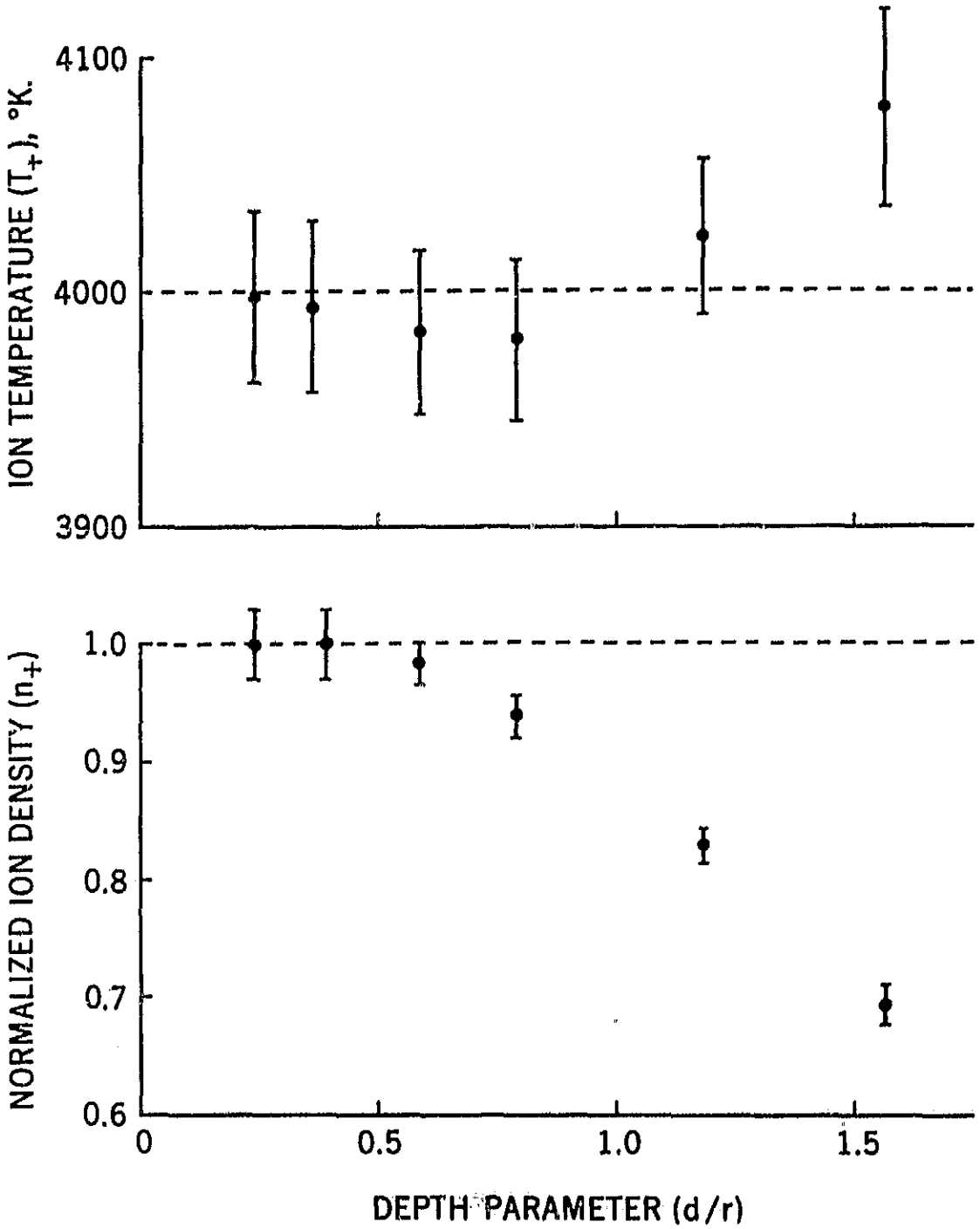
4100
4000
3900
ION TEMPERATURE (T_+), °K.
1.0
0.9
0.8
0.7
0.6
NORMALIZED ION DENSITY (n_+)
0
0.5
1.0
1.5
DEPTH PARAMETER (d/r)

Figure 5.

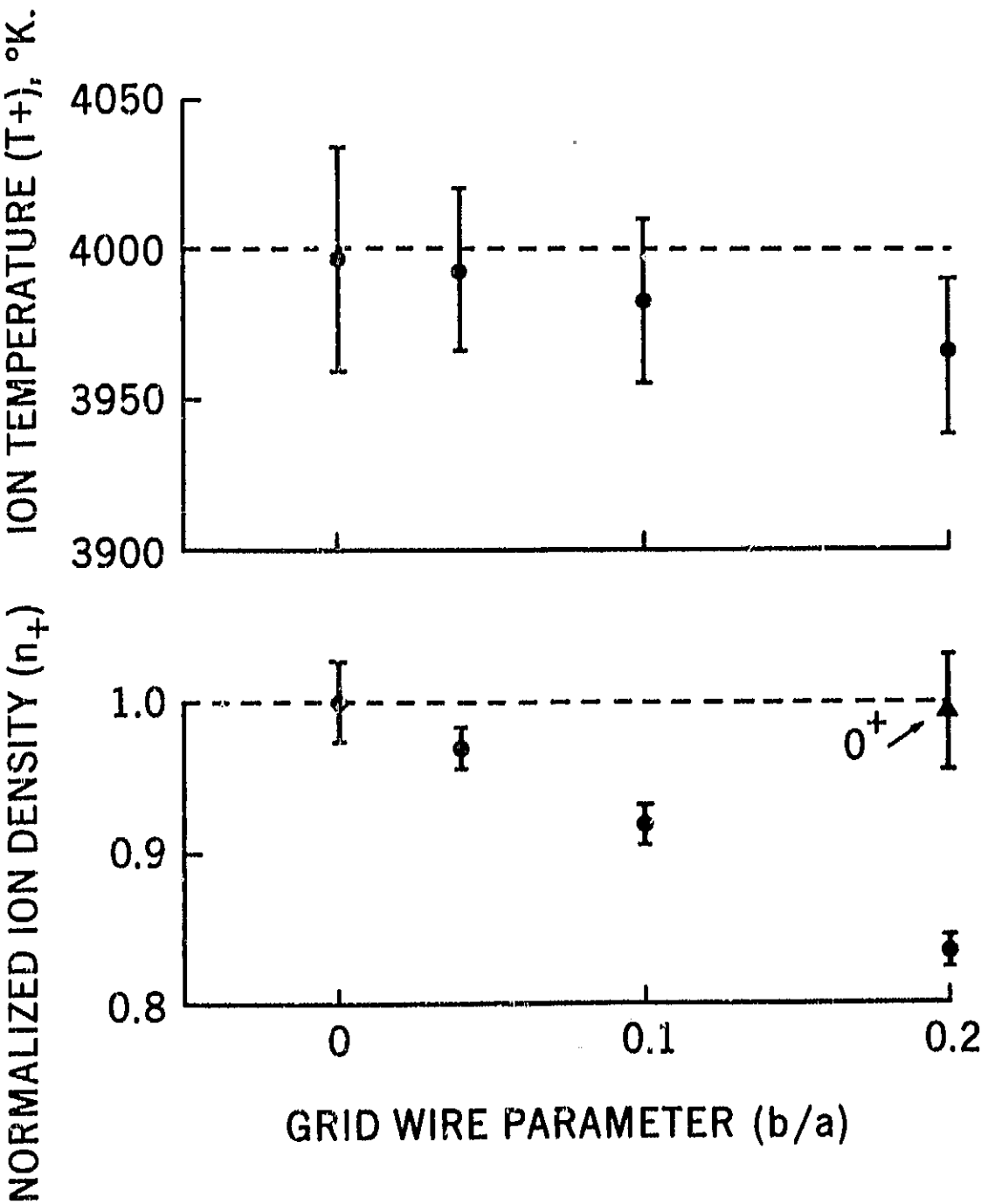
ION TEMPERATURE (T+), °K.
4050
4000
3950
3900
NORMALIZED ION DENSITY (n+)
1.0
0.9
0.8
0+
0
0.1
0.2
GRID WIRE PARAMETER (b/a)

Figure 6.